Improved thermoelectric performance of Bi_2Se_3 alloyed Bi_2Te_3 thin films *via* low pressure chemical vapour deposition

Daniel W. Newbrook[a], Stephen P. Richards[b], Victoria K. Greenacre[b], Andrew L. Hector[b], William Levason[b], Gillian Reid[b], C. H. (Kees) de Groot[a] and Ruomeng Huang*[a]

[a]*School of Electronics and Computer Science, University of Southampton, Southampton, United Kingdom*

[b]*School of Chemistry, University of Southampton, Southampton, United Kingdom*

ABSTRACT

Thermoelectric generators are attractive for autonomous sensor systems where regular battery replacement would not only cause an increase in the maintenance costs and discontinuity in the operation, but also destroy the concept of a truly autonomous system. Micro-thermoelectric generators utilise thin films of material for energy harvesting which can greatly reduce the amount of material used, which is especially important for rare elements such as tellurium. Thin films of Bi_2Te_3 were successfully prepared via a single source precursor CVD method. The thermoelectric performance of these films is improved by alloying a Bi_2Se_3 precursor to deposit ternary $Bi_2Te_{3-x}Se_x$. The composition of the ternary system is tuned to optimise the combination of carrier concentration and mobility to give a three-fold enhancement of the thermoelectric power factor at 300K, and six-fold enhancement at 500K, with respect to Bi_2Te_3. This improvement from the substitution of Te with Se is believed to be due to donor effects, as well as point defects caused by this substitution.

Keywords: Thin films, Chemical vapour deposition, Point defect, Thermoelectric

1. Introduction

Micro-thermoelectric generators (μTEGs) are solid-state devices, based on the Seebeck effect, that are formed by connecting an n-type doped material electrically in series and thermally in parallel to a p-type doped material across a temperature differential, allowing current flow through the two materials. They can transform waste heat produced daily in our society into electricity while offering high reliability, long lifetimes, no maintenance, and solid-state operation. They have the potential to provide a sustainable power solution to microelectronics devices (e.g. sensor nodes in the Internet of Things (IoT)) and on-chip hot spot cooling of microprocessors [1,2]. However, improvements in both the thermoelectric material properties and device efficiency are required to make them useful for sustainable energy-harvesting and cooling applications.

Improvement of thermoelectric material properties lies in the improvement of the figure of merit ZT ($ZT = S^2\sigma/(\kappa_{el} + \kappa_{la})$, where S is the Seebeck coefficient, σ is the electrical conductivity, κ_{el} is the electronic contribution to thermal conductivity, and κ_{la} is the lattice contribution to thermal conductivity). An effective strategy for improving the power factor to achieve high ZT values is by tuning the carrier concentration as S, σ and k_{el} are heavily dependent on it [3,4]. Depending on their effective working temperatures, thermoelectric materials can be separated into high-temperature, mid-temperature, and room-temperature applications [5–7]. The most realistic temperature range for energy harvesting using μTEG is near room temperature, and the most popular materials reported are based on Bi_2Te_3 and Sb_2Te_3 due to their high room-temperature ZT values [8–10].

Commercial acceptance of chalcogenide-based micro-TEGs can be restricted due to the scarcity of tellurium. This has sparked a considerable effort to search for alternative, more sustainable TE materials, including silicides [11] and oxides [12–14], as well as using other techniques such as nano-structuring to improve material performance [1]. However, replacements are not readily forthcoming and Bi_2Te_3 remains one of the most promising materials for low-temperature waste heat recovery. An alternative to the replacement of Bi_2Te_3 is to reduce the volume of material required to achieve the same or higher performance. For example, partial replacement of the low natural abundance of tellurium by selenium contributes strongly to a sustainable thermoelectric solution [15–17]. Several groups have produced ternary $Bi_2Te_{3-x}Se_x$ thin films *via* electrodeposition [18–25], pulsed laser deposition [26], sputtering [27,28], and thermal evaporation [29–31]. Electrodeposition allows spatial selective deposition, but the thermoelectric properties from room temperature deposition are often inferior and post-deposition annealing is normally required for improved performance [18]. The other deposition techniques can produce good quality materials using dual or multiple sources, but the ternary composition control can be challenging, and substrate-selective deposition has not been achieved using those techniques.

Chemical vapour deposition (CVD) allows for the production of superior quality thin films with better conformity, coverage, and stoichiometric control compared with sputtering. Conventional deposition of binary or ternary compounds requires the

use of multiple precursor systems [32], however recent work in single-source precursors (SSPs) is a promising alternative, allowing ease of handling and atom efficiency without compromising on stoichiometry or morphological control. We have previously demonstrated the viabilities of using SSPs to deposit high-quality binary (e.g. $SnSe_2$, $TiSe_2$, Bi_2Te_3, and Sb_2Te_3) and ternary ($Bi_2(Se_{1-x}Te_x)_3$ and $(Bi_{1-y}Sb_y)_2Te_3$) chalcogenides by using appropriate combinations of precursors [33–37]. The possibility of selective deposition of oriented films onto defined regions of lithographically patterned substrates has also been realised using these types of precursors [38], paving the way for their application in functional semiconductor devices.

In this work, we report the temperature-dependent thermoelectric properties of *n*-type $Bi_2Te_{3-x}Se_x$ thin films deposited by low-pressure CVD. The resultant films demonstrate high purity with thermoelectric properties comparable to state-of-the-art values. The thermoelectric properties are further improved through carrier concentration tuning by alloying with Bi_2Se_3 using analogue single-source precursors. This leads to a three-fold enhancement of the power factor at 300K and a significant reduction of tellurium consumption. The selective deposition behaviour of this CVD approach on thermoelectric generator structures is demonstrated which facilitates the efficient integration of micro-thermoelectric generator.

2. Materials and methods

2.1. Single source precursor synthesis

Single-source precursor $BiCl_3(Te^nBu_2)_3$ was synthesized for the deposition of Bi_2Te_3 thin films. Ternary $Bi_2Te_{3-x}Se_x$ precursors were prepared by an appropriate combination of the $BiCl_3(Te^nBu_2)_3$ with its selenium analogue, $BiCl_3(Se^nBu_2)_3$, at various ratios to achieve different film compositions. More information about the precursor synthesis can be found in our previous work [37].

2.2. LPCVD of Bi_2Te_3 and $Bi_2Te_{3-x}Se_x$

For a typical deposition, both the precursor and substrates were loaded into a closed-end quartz tube in a glove-box. The precursor, *ca.* 70 mg, was placed at the closed end and several SiO_2-coated silicon substrates were positioned end-to-end near the precursor. After loading the substrates, the tube was set to the designated deposition temperature in a furnace such that the precursor was outside the heated zone; the tube was evacuated, heated to the set temperature under 6.67 Pa and the furnace was allowed to stabilise. The tube position was subsequently adjusted so that the precursor was moved gradually towards the hot zone until evaporation was observed. In this work, the furnace temperature was fixed at 525°C to ensure a similar deposition temperature. The actual reaction temperature was characterised by temperature profiling along the tube and identified to be 400±10°C. The tube remained unmoved until the precursor had completely evaporated (no residual precursor remained), i.e. *ca.* 1–3 h. After this, the tube was cooled to room temperature and transferred to the glove box where the tiles were removed and stored under an N_2 atmosphere prior to analysis.

2.3. Thin film characterisation

Scanning electron microscopy (SEM) was performed using a Zeiss EVO LS 25 with an accelerating voltage of 10 kV, and energy-dispersive X-ray (EDX) data were obtained with an Oxford INCAx-act X-ray detector. High-resolution SEM measurements were carried out with a field emission SEM (Jeol JSM 7500F) at an accelerating voltage of 2 kV. X-ray diffraction (XRD) measurements were carried out using a Rigaku Smartlab diffractometer with a 9 kW Cu-Ka source, a parallel line focus incident beam, and a DTex250 1D detector. Analysis and refinement of XRD results were performed in the SmartLab Studio software suite. X-ray photoelectron spectroscopy (XPS) data were obtained using a ThermoScientific Theta Probe System with Al–Kα radiation (photon energy= 1486.6 eV). XPS depth profile was performed by using an Ar ion gun at a beam voltage of 3 kV on a 2 × 2 mm raster area. Raman scattering spectra of the deposited films were measured at room temperature on a Renishaw InVia Micro Raman Spectrometer using a helium–neon laser with a wavelength of 633 nm. The incident laser power was adjusted to be *ca.*1 mW for all samples.

The in-plane electrical conductivity (σ) and Seebeck coefficient (S) were simultaneously measured on a commercial Joule Yacht Thin-film Thermoelectric Parameter Test System (MRS-3L). The system was calibrated using Nickel foil reference standard and the measurement accuracy was found to be within 5%. The Hall coefficient (R_H) was determined at 300 K on a Nanometrics HL5500PC instrument using a van der Pauw configuration. The carrier concentration (n_H) and in-plane mobility (μ_H) were computed according to $n_H = 1/eR_H$ and $\mu_H = \sigma R_H$, respectively.

3. Results and discussion

Cross-sectional SEM images (Fig. 1a-1e) of the samples show that all $Bi_2Te_{3-x}Se_x$ ternary films are polycrystalline and continuous with good coverage across the substrate. Hexagonal crystallites are clearly visible in the top-view SEM images

(Fig. S1), although the orientations are different. Film thicknesses of all five films are slightly different, which is possibly due to the different precursor combinations used for each composition. The composition of each film was investigated by EDX and the spectra are shown in Fig. 1f. The selenium peak at 1.3 keV increases monotonically with increasing selenium content *x* from 0 to 1.3. The relative atomic percentages are shown in Table S1. This variation of composition is further confirmed by XPS measurement (Fig. S2).

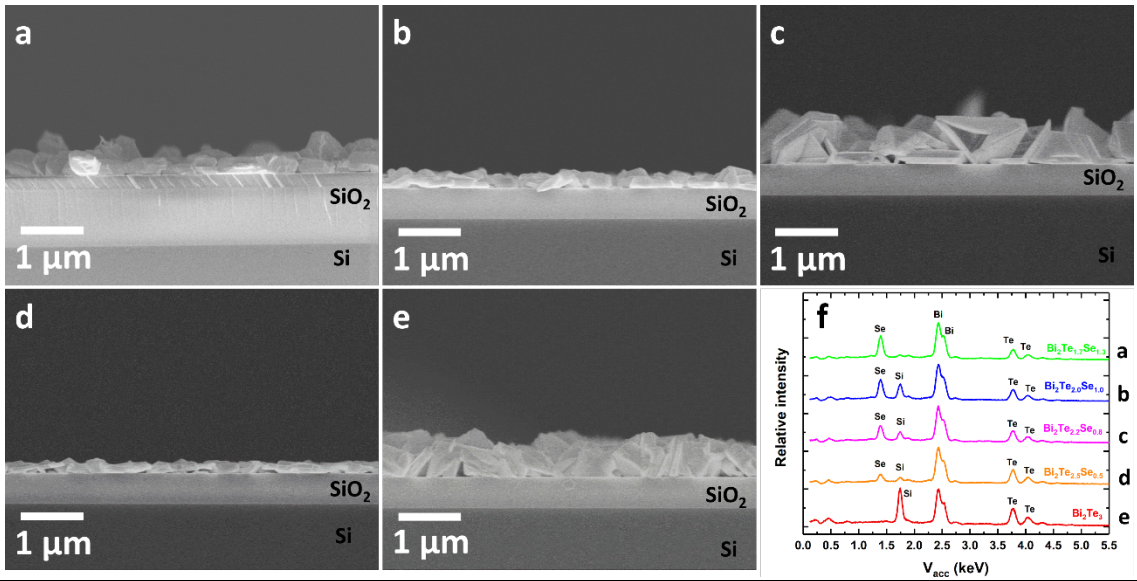

Fig. 1 Cross-sectional SEM images showing the morphologies of $Bi_2Te_{3-x}Se_x$ (a–e x=1.3, 1.0, 0.8, 0.5, and 0) films deposited by LPCVD onto SiO_2-coated silicon substrates and their corresponding EDX spectra (f). Appearance of underlying Si peak depends on thickness of the film at the exact spot an does not influence extracted composition.

Grazing incidence XRD analysis (Fig. 2a) on these films reveal that they are all isostructural with no other phases. The preferred in-plane orientation of some films (x = 0, 0.5, 1.0) as deduced from their enhancement of 006 peaks are consistent with the SEM images in Fig. 1 with alignment resulting in significantly thinner films. A shift of the 015 peak position with increasing Se alloying is highlighted in Fig. 2b. The lattice parameters (a, c) of all five compositions were obtained by refining the collected XRD data against the Bi_2Te_3 phases from ICSD [39]. Linear decreases of both a and c with increasing Se content are observed (Fig. 2c), consistent with Vegard's law, implying the well-distributed solid solutions of the ternary $Bi_2Te_{3-x}Se_x$. The vibrational properties of the as-deposited $Bi_2Te_{3-x}Se_x$ thin films were also investigated by Raman spectroscopy with spectra shown in Fig. S3a. Two vibrational modes, E_g^2 (in-plane) and A_{1g}^2 (out-of-plane), are present in the five films. Both modes shift progressively to higher wavenumbers with increasing Se content (Fig. S3b) which is consistent with the XRD result.

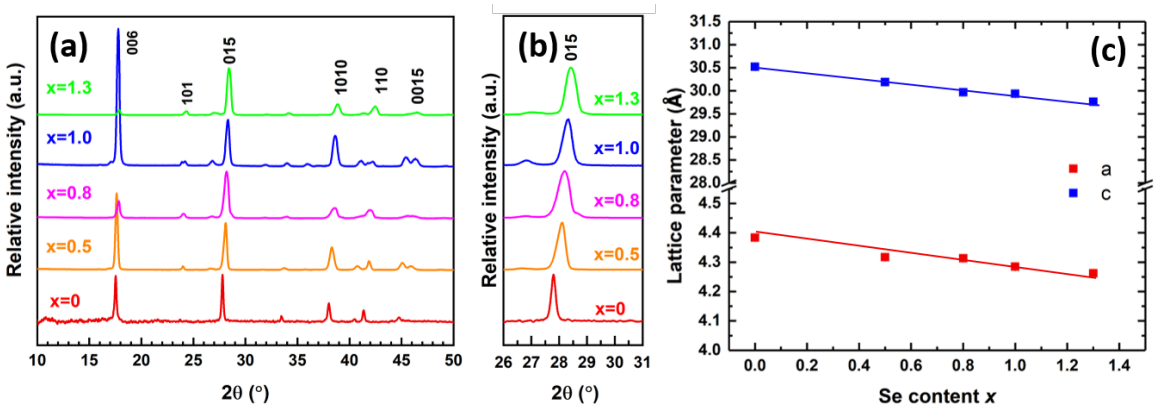

Fig. 2 (a) XRD patterns of as-deposited $Bi_2Te_{3-x}Se_x$ films with x ranging from 0 to 1.3; (b) expanded XRD patterns showing the systematic shift of the 015 peak; (c) refined lattice parameters as a function of the Se content for different as-deposited $Bi_2Te_{3-x}Se_x$ films.

Fig. 3a shows the room temperature carrier concentration n_H and mobility μ_H of the $Bi_2Te_{3-x}Se_x$ thin films as a function of Se content. As-deposited Bi_2Te_3 demonstrates n-type conductivity with a high carrier concentration, indicating a large concentration of anion vacancies $V_{Te}^{\cdot\cdot}$ which has already surpassed that of antisite defects (Bi_{Te}') leading to a donor-like effect whereby the number of free electrons increases by these defects [40]. This donor-like effect can be explained by the Bi atom diffusing from a Te site back to their original sublattice site, creating extra Te vacancies and excess electrons. Substitution of Te more electronegative or smaller atoms of the same valence on the anion site (i.e. Se) tends to drive the Bi-Te system towards electron-like (n-type) conduction [40]. This is due to the lower vacancy formation energy of the Bi-Se system than that of the Bi-Te system, which increases the concentration of anion vacancies [40,41]. However, a decrease in the electron concentration is then observed when the Se content varies from 0.5 to 0.8. This could be explained by the suppression of the donor-like effect through an initial decrease in the antisite effect [40]. This donor-like effect is re-enhanced when $x > 1$, represented by the further increased n_H. We observed this pattern for multiple depositions of the same composition. Similar results have also been observed in previous reports [41,42]. Although Fig. 3a shows no clear correlation between carrier concentration and Se content, the Se content affects these defect processes and thus causes the carrier concentration and mobility to change with Se content. Also to note is that although this defects-related model can explain the trends seen in Fig. 3a, more works are required to verify it. The as-deposited films are also characterized by relatively low electron mobilities ($< 10\,cm^2/Vs$), suggesting strong scattering effects in the films. These scattering effects are likely due to the high concentration of ionized impurities (e.g. $V_{Te}^{\cdot\cdot}$ and $V_{Se}^{\cdot\cdot}$) in the film concentration of anion vacancies which reduces the carrier relaxation time [3,43]. Ionized impurity atoms residing in the lattice will act as scattering centers to carriers. Fig. 3b shows the electron mobility as a function of crystal size, obtained from the XRD spectra using Scherrer equation ($\tau = K\lambda/\beta \cos\theta$). An increase of μ_H is observed with increasing crystal size, which could be associated with the reduction of the grain-boundary scattering [3]. This increase in crystal size correlates also to an increase in film thickness. The effect of crystal orientation on the mobility reported by other works is not observed in our films [44].

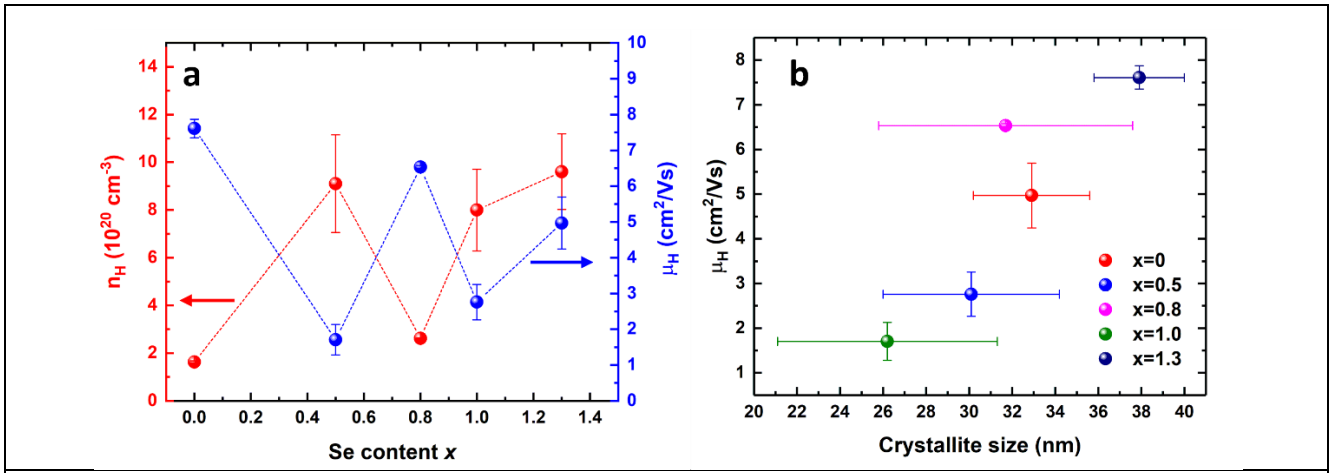

Fig. 3 (a) Room temperature carrier concentration and mobility of the as-deposited $Bi_2Te_{3-x}Se_x$ films with x ranging from 0 to 1.3. (b) Mobility of the as-deposited $Bi_2Te_{3-x}Se_x$ films as a function of crystallite size.

The electrical properties of the Bi_2Te_3 thin film can be optimized *via* Bi_2Se_3 alloying using our CVD approach. The temperature-dependent electrical conductivities of the $Bi_2Te_{3-x}Se_x$ films are presented in Fig. 4a. All films demonstrate negative temperature dependence, indicative of semi-metallic transport behaviour [45]. Bi_2Se_3 alloying increases the σ, especially after the donor-like effect is re-enhanced when $x > 0.8$ as shown in Fig. 4b. The temperature-dependent Seebeck coefficients are shown in Fig. 4c. It is clear that all thin films possess negative Seebeck coefficients, confirming their n-type conductivity. Higher S values are observed at $x = 0.8$, which is consistent with the low n_H of this film (Fig. 4d).

To further shed light on the electrical transport mechanism, the Seebeck coefficient versus carrier concentration (Pisarenko plot) at 300K is plotted in Fig. 4e. A simple electron transport model is used to calculate the dotted lines, which serve as guidelines. The model can be written as:

$$S = \frac{8\pi^2 k_B^2}{3eh^2}\left(\frac{\pi}{3n}\right)^{2/3} m^* T$$

where k_B is the Boltzmann constant, h the Planck constant, and m^* the effective mass [46]. It assumes a single parabolic band and approximates energy-independent carrier scattering in degenerate semiconductors [47]. All films are characterized by high effective mass values, which is consistent with the low carrier mobility observed in Fig. 3a. Variation of effective masses (from $1.5m_0$ to $3.5m_0$) of the five $Bi_2Te_{3-x}Se_x$ films is also observed, which reflects the variation of the carrier mobility. However, it should be noted that the true value of effective mass is open to question given the complexity of the actual physical situation. The assumption of an energy independent scatting could be incorrect in which case a scattering constant λ should be adopted in the above equation to represent the energy dependence of the electronic scattering distance:

$$S = \frac{8\pi^2 k_B^2}{3eh^2}\left(\frac{\pi}{3n}\right)^{2/3} m^* T(1+\lambda)$$

λ is in the range between 0 and 2 where $\lambda = 0$ implies lattice (acoustic phonon) scattering and $\lambda = 2$ corresponds to ionized impurity scattering [48]. If the ionized impurity scattering (which is likely to contribute at least partially to the scattering of our films due to the high carrier concertation) was taken into account, the effective mass for our Bi_2Te_3 should be in the range of ~1.17 to 3.5m0. Similar discussions have also been reported in other heavily doped films such as lanthanum telluride cerium sulphide [48–50].

The power factors of the $Bi_2Te_{3-x}Se_x$ films are shown in Fig. 4f. As a result of enhanced electrical conductivity due to Bi_2Se_3 alloying, a significant increase of power factor is obtained, in particular for $x = 1.3$ where three-fold and six-fold enhancements of power factor are observed compared with $x = 0$ at 300K and 500K, respectively. The maximum power factor of 7.6 $\mu W/cmK^2$ at 525K is shown in Fig. 4f. Kim *et al.* report a room temperature power factor of 11.5 $\mu W/cmK^2$ for their as-deposited electrodeposited films [18]. However, the compositions of those films reported were still quite high in tellurium with $x = 0.15$. For sputtered films, Chen *et al.* reported a room temperature power factor of around 4.4 $\mu W/cmK^2$ for their films [27].

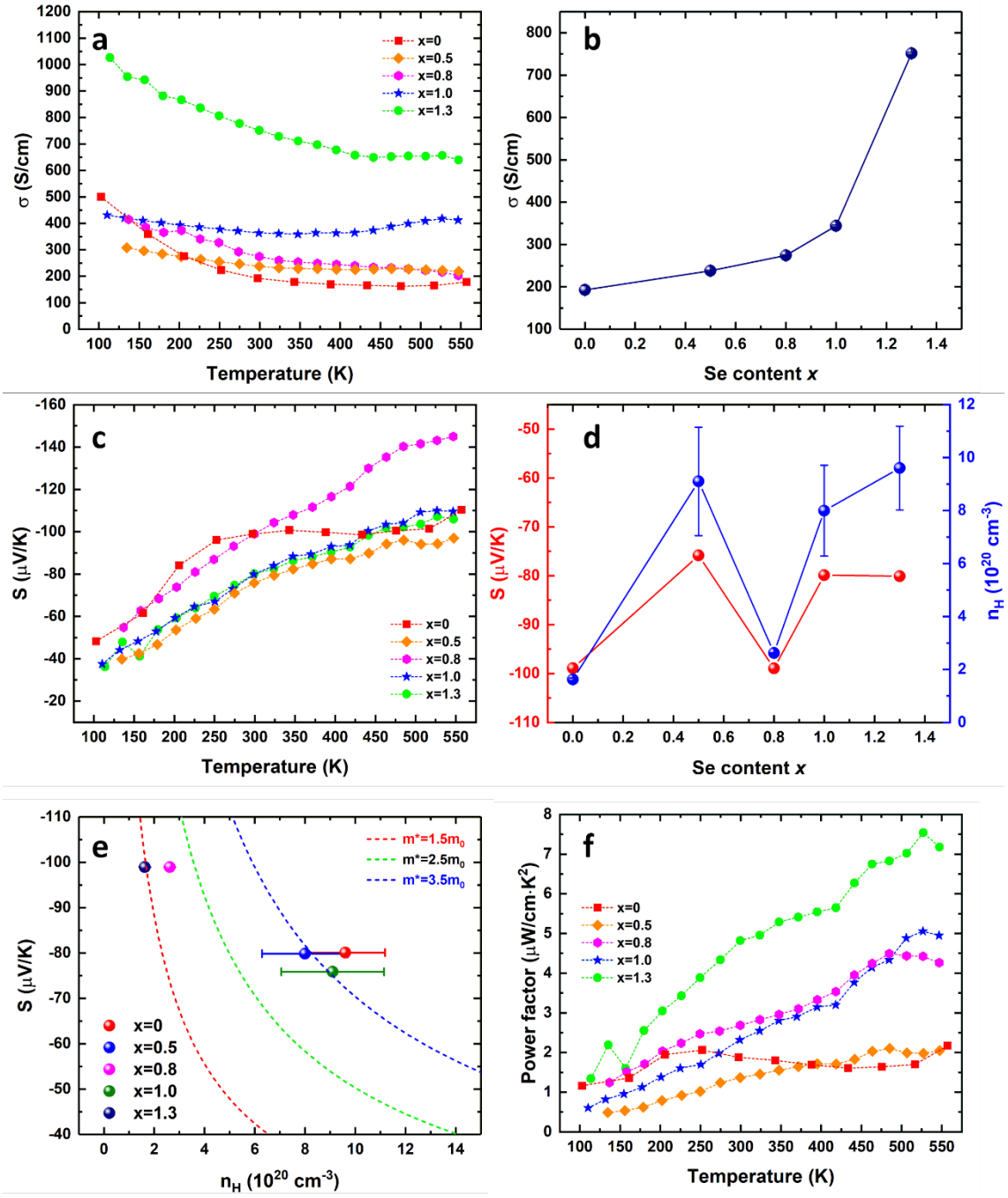

Fig. 4 (a) Temperature dependent in-plane electrical conductivity of the as-deposited $Bi_2Te_{3-x}Se_x$ films with x ranging from 0 to 1.3. (b) Room temperature electrical conductivity as a function of Se content. (c) Temperature dependent in-plane Seebeck coefficient of the as-deposited $Bi_2Te_{3-x}Se_x$ films with x ranging from 0 to 1.3. (d) Room temperature Seebeck coefficient and carrier concentration as a function of Se content. (e) Room temperature Seebeck coefficient as-deposited $Bi_2Te_{3-x}Se_x$ films as a function of the carrier concentration (Pisarenko plot), the dotted lines represent the values calculated for $m^* = 1.5, 2.5\ and\ 3.5\ m_e$. (f) Temperature dependent in-plane power factor of the as-deposited $Bi_2Te_{3-x}Se_x$ films with x ranging from 0 to 1.3.

Measurement of thermal conduction properties of thin films is extremely challenging and often prone to error. Here we estimate the total thermal conductivity by assuming a constant lattice contribution of 0.5 W/mK. We believe this is a relatively conservative estimation giving the small size of our crystals when compared to similar work that shows a lattice thermal conductivity of less than 0.3 W/mK for Bi_2Te_3 with similar crystallite sizes [51]. We would also expect the value to decrease

with alloying. This would help to reduce the lattice thermal conductivity by enhancing phonon-scattering [3,52,53]. The electrical contribution of the thermal conductivity (k_{el}) is calculated (Fig. S4) using the Wiedemann-Franz law ($k_{el} = L\sigma T$), where L is the Lorenz number and was calculated by adopting an empirical equation proposed by Snyder *et al.* [54]. The temperature-dependent ZT values of the $Bi_2Te_{3-x}Se_x$ films based on the estimated thermal conductivity are presented in Fig. 5. Two optimised compositions are identified at $x = 0.8$ and $x = 1.3$, owing to their high Seebeck coefficient and electrical conductivity, respectively.

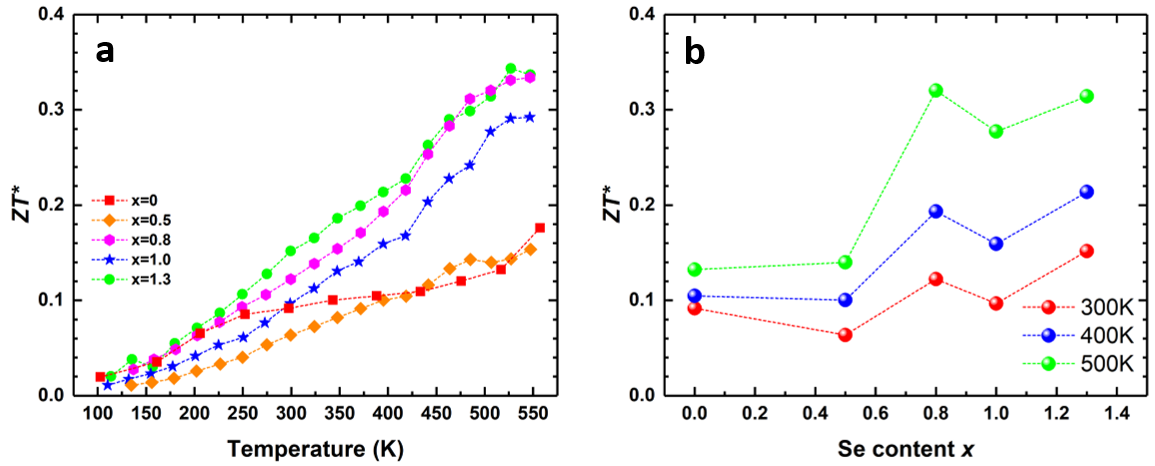

Fig. 5 (a) Estimated temperature dependent ZT of the as-deposited $Bi_2Te_{3-x}Se_x$ films with x ranging from 0 to 1.3. (b) ZT as a function of Se content at 300, 400 and 500K.

One advantage of this CVD approach is the selective deposition behaviour in which thermoelectric materials can be selectively deposited into conductive patterned surfaces (e.g. TiN) [35]. Here we demonstrate this unique behaviour can also be achieved in a thermoelectric generator pattern as shown in Fig. 6. All the exposed TiN surfaces (red square) are fully filled with Bi_2Te_3, as evidenced by the EDX mapping in Fig. 6b-6d, with very little deposition observed outside the areas on the SiO_2 surface. This forms the n-leg regions without the need for patterning and etching the material. A full thermoelectric generator can be achieved by further selective deposition of p-type TE material in the blue regions.

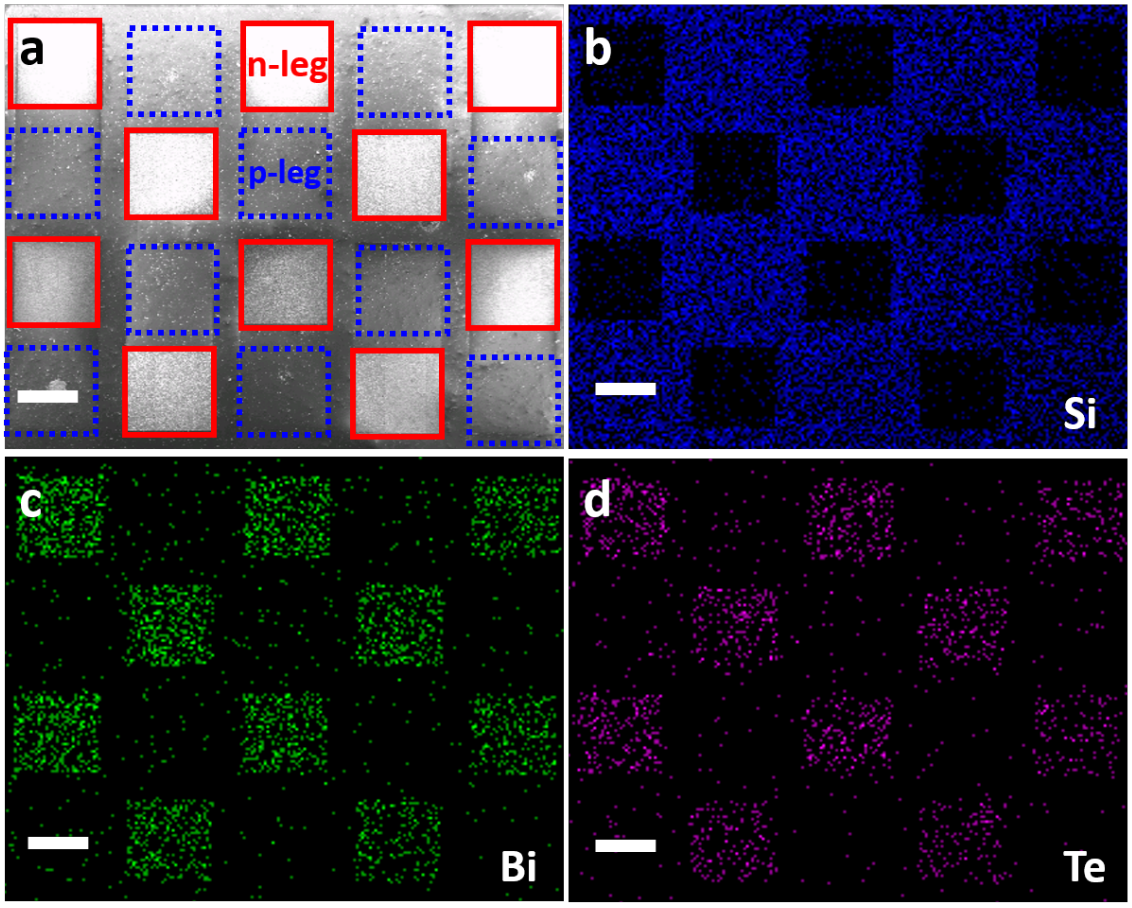

Fig. 6 (a) SEM image (a) and EDX element maps (b–d) confirming the selective deposition of Bi_2Te_3 onto a TiN/SiO_2 patterned substrate for thermoelectric generator fabrication. The scale bar is 200 µm.

4. Conclusions

We have demonstrated the deposition and thermoelectric properties of n-type $Bi_2Te_{3-x}Se_x$ with a range of x from 0-1.3 by mixing Bi_2Te_3 and Bi_2Se_3 single source precursor-based CVD. By tuning the $Bi_2Te_{3-x}Se_x$ composition, the carrier concentration and mobility can be optimized to give a maximum power factor of 7.6 $\mu W/cmK^2$ for a composition of $Bi_2Te_{1.7}Se_{1.3}$, at 550K, leading to an estimated ZT of 0.34. This change in carrier concentration is believed to be from a donor-like effect due to the difference in electronegativity and size between Bi-Te, and Bi-Se. The unique selective deposition behavior of this system has also been shown to be successful.

Acknowledgements

We thank the STFC for funding (ST/L003376/1 and ST/P00007X/1). We also gratefully acknowledge funding for thin film diffraction and NMR instrumentation from the EPSRC through EP/K00509X, EP/K009877/1 and EP/K039466/1. DWN would like to thank both BAE and EPSRC for funding the iCASE studentship. All data supporting this study are openly available from the University of Southampton repository at DOI: https://doi.org/10.5258/SOTON/D1366

References

[1] H. Alam, S. Ramakrishna, A review on the enhancement of figure of merit from bulk to nano-thermoelectric materials, Nano Energy. 2 (2013) 190–212. https://doi.org/10.1016/j.nanoen.2012.10.005.

[2] S.H. Choday, M.S. Lundstrom, K. Roy, Prospects of Thin-Film Thermoelectric Devices for Hot-Spot Cooling and On-Chip Energy Harvesting, IEEE Trans. Components, Packag. Manuf. Technol. 3 (2013) 2059–2067. https://doi.org/10.1109/TCPMT.2013.2273873.

[3] T. Zhu, Y. Liu, C. Fu, J.P. Heremans, J.G. Snyder, X. Zhao, Compromise and Synergy in High-Efficiency Thermoelectric Materials, Adv. Mater. 29 (2017) 1605884. https://doi.org/10.1002/adma.201605884.

[4] I.T. Witting, T.C. Chasapis, F. Ricci, M. Peters, N.A. Heinz, G. Hautier, G.J. Snyder, The Thermoelectric Properties of Bismuth Telluride, Adv. Electron. Mater. 5 (2019) 1800904. https://doi.org/10.1002/aelm.201800904.

[5] Q. Zhang, R. Zhai, T. Fang, K. Xia, Y. Wu, F. Liu, X. Zhao, T. Zhu, Low-cost p-type Bi2Te2.7Se0.3 zone-melted thermoelectric materials for solid-state refrigeration, J. Alloys Compd. 831 (2020) 154732. https://doi.org/10.1016/j.jallcom.2020.154732.

[6] Y. Wu, Q. Zhang, F. Liu, T. Fang, T. Zhu, X. Zhao, Scattering Mechanisms and Compositional Optimization of High-Performance Elemental Te as a Thermoelectric Material, Adv. Electron. Mater. 6 (2020) 1–11. https://doi.org/10.1002/aelm.202000038.

[7] L. Pan, W.-D. Liu, J.-Y. Zhang, X.-L. Shi, H. Gao, Q. Liu, X. Shen, C. Lu, Y.-F. Wang, Z.-G. Chen, Synergistic effect approaching record-high figure of merit in the shear exfoliated n-type Bi2O2-2xTe2xSe, Nano Energy. 69 (2020) 104394. https://doi.org/10.1016/j.nanoen.2019.104394.

[8] G.J. Snyder, E.S. Toberer, Complex thermoelectric materials, Nat. Mater. 7 (2008) 105–114. https://doi.org/10.1038/nmat2090.

[9] J. Feng, W. Zhu, Z. Zhang, L. Cao, Y. Yu, Y. Deng, Enhanced Electrical Transport Properties via Defect Control for Screen-Printed Bi 2 Te 3 Films over a Wide Temperature Range, ACS Appl. Mater. Interfaces. 12 (2020) 16630–16638. https://doi.org/10.1021/acsami.0c01049.

[10] R. Venkatasubramanian, E. Siivola, T. Colpitts, B. O'Quinn, Thin-film thermoelectric devices with high room-temperature figures of merit, Nature. 413 (2001) 597–602. https://doi.org/10.1038/35098012.

[11] G. Kim, H. Shin, J. Lee, W. Lee, A Review on Silicide-Based Materials: Thermoelectric and Mechanical Properties, Met. Mater. Int. (2020). https://doi.org/10.1007/s12540-020-00609-9.

[12] Y. Yin, B. Tudu, A. Tiwari, Recent advances in oxide thermoelectric materials and modules, Vacuum. 146 (2017) 356–374. https://doi.org/10.1016/j.vacuum.2017.04.015.

[13] F.P. Zhang, Q.M. Lu, X. Zhang, J.X. Zhang, First principle investigation of electronic structure of CaMnO3 thermoelectric compound oxide, J. Alloys Compd. 509 (2011) 542–545. https://doi.org/10.1016/j.jallcom.2010.09.102.

[14] F.P. Zhang, Q.M. Lu, X. Zhang, J.X. Zhang, Electrical transport properties of CaMnO3 thermoelectric compound: a theoretical study, J. Phys. Chem. Solids. 74 (2013) 1859–1864. https://doi.org/10.1016/j.jpcs.2013.07.019.

[15] B.-S. Kim, G. Lee, H.-J. Lim, J. Jang, J.E. Lee, B.-K. Min, S.-J. Joo, S. Park, B. Ryu, H.S. Lee, Thermoelectric Properties of Off-Stoichiometric Bi2Te2Se Compounds, J. Electron. Mater. (2020). https://doi.org/10.1007/s11664-020-08258-9.

[16] M.S. Shalaby, H.M. Hashem, N.M. Yousif, H.A. Zayed, A. Sotelo, L.A. Wahab, Preparation, structural characteristics and optical parameters of the synthesized nano-crystalline sulphur-doped Bi2Te2.85Se0.15 thermoelectric materials, J. Mater. Sci. Mater. Electron. 31 (2020) 10612–10627. https://doi.org/10.1007/s10854-020-03611-4.

[17] T. Liu, W. Zhu, R. Wang, S. Li, Y. Xiao, Improvement of thermoelectric performance of Bi 2 Te2.7Se0.3 via grain boundary engineering with melting KOH, Funct. Mater. Lett. 12 (2019) 1950082. https://doi.org/10.1142/S1793604719500826.

[18] J. Kim, K.H. Lee, S.W. Kim, J.-H. Lim, Potential-current co-adjusted pulse electrodeposition for highly (110)-oriented Bi2Te3-Se films, J. Alloys Compd. 787 (2019) 767–771. https://doi.org/10.1016/j.jallcom.2019.01.301.

[19] Z.G. Zou, K.F. Cai, S. Chen, Z. Qin, Pulsed electrodeposition and characterization of Bi2Te3−ySey films, Mater. Res. Bull. 47 (2012) 3292–3295. https://doi.org/10.1016/j.materresbull.2012.07.036.

[20] S. Michel, S. Diliberto, N. Stein, B. Bolle, C. Boulanger, Characterisation of electroplated Bi 2(Te 1-xSe x) 3 alloys, J. Solid State Electrochem. 12 (2008) 95–101. https://doi.org/10.1007/s10008-007-0362-9.

[21] L. Bu, W. Wang, H. Wang, Effect of the substrate on the electrodeposition of Bi2Te3−ySey thin films, Mater. Res. Bull. 43 (2008) 1808–1813. https://doi.org/10.1016/j.materresbull.2007.07.002.

[22] C. Schumacher, K.G. Reinsberg, R. Rostek, L. Akinsinde, S. Baessler, S. Zastrow, G. Rampelberg, P. Woias, C. Detavernier, J.A.C. Broekaert, J. Bachmann, K. Nielsch, Optimizations of Pulsed Plated p and n-type Bi 2 Te 3 -Based Ternary Compounds by Annealing in Different Ambient Atmospheres, Adv. Energy Mater. 3 (2013) 95–104. https://doi.org/10.1002/aenm.201200417.

[23] Y. Ma, W. Wijesekara, A.E.C. Palmqvist, Electrochemical Deposition and Characterization of Thermoelectric Ternary (Bi x Sb1−x)2Te3 and Bi2(Te1−y Se y)3 Thin Films, J. Electron. Mater. 41 (2012) 1138–1146. https://doi.org/10.1007/s11664-011-1790-y.

[24] S. Michel, N. Stein, M. Schneider, C. Boulanger, J.M. Lecuire, Optimization of chemical and electrochemical parameters for the preparation of n-type Bi2Te2.7Se0.3 thin films by electrodeposition, J. Appl. Electrochem. 33 (2003) 23–27. https://doi.org/10.1023/A:1022914615625.

[25] W.-S. Kang, W.-C. Chou, W.-J. Li, T.-H. Shen, C.-S. Lin, Electrodeposition of Bi2Te3-based p and n-type ternary thermoelectric compounds in chloride baths, Thin Solid Films. 660 (2018) 108–119. https://doi.org/10.1016/j.tsf.2018.06.001.

[26] P.H. Le, S.-P. Chiu, S.-R. Jian, C.W. Luo, J.-Y. Lin, J.-J. Lin, K.H. Wu, M. Gospodinov, Nanomechanical, structural, and transport properties of Bi3Se2Te thin films, J. Alloys Compd. 679 (2016) 350–357. https://doi.org/10.1016/j.jallcom.2016.03.226.

[27] P.-J. Chen, C.-N. Liao, Thermoelectric transport properties of Bi–Te based thin films on strained polyimide substrates, Appl. Phys. Lett. 105 (2014) 133903. https://doi.org/10.1063/1.4897302.

[28] K.M. Liou, C.N. Liao, Electric current enhanced defect elimination in thermally annealed Bi–Sb–Te and Bi–Se–Te thermoelectric thin films, J. Appl. Phys. 108 (2010) 053711. https://doi.org/10.1063/1.3477184.

[29] A.M. Adam, E.M.M. Ibrahim, L. V. Panina, P. Petkov, Optical And Thermoelectric Properties Of Nanocrystalline Bi 2 (Se 1-x Te x) 3 Films, Nanoscale Microscale Thermophys. Eng. 22 (2018) 21–38. https://doi.org/10.1080/15567265.2017.1363835.

[30] A.M. Adam, A. El-Khouly, E. Lilov, S. Ebrahim, Y. Keshkh, M. Soliman, E.M. El Maghraby, V. Kovalyo, P. Petkov, Ultra thin bismuth selenide-bismuth telluride layers for thermoelectric applications, Mater. Chem. Phys. 224 (2019) 264–270. https://doi.org/10.1016/j.matchemphys.2018.12.034.

[31] L.I. Soliman, M.M. Nassary, H.T. Shaban, A.S. Salwa, Influence of Se on the electron mobility in thermal evaporated Bi2(Te1−xSex)3 thin films, Vacuum. 85 (2010) 358–364. https://doi.org/10.1016/j.vacuum.2010.06.003.

[32] C.W. Lee, G.H. Kim, J.W. Choi, K.-S. An, J.-S. Kim, H. Kim, Y.K. Lee, Improvement of thermoelectric properties of Bi 2 Te 3 and Sb 2 Te 3 films grown on graphene substrate, Phys. Status Solidi - Rapid Res. Lett. 11 (2017) 1700029. https://doi.org/10.1002/pssr.201700029.

[33] C.H. (Kees) de Groot, C. Gurnani, A.L. Hector, R. Huang, M. Jura, W. Levason, G. Reid, Highly Selective Chemical Vapor Deposition of Tin Diselenide Thin Films onto Patterned Substrates via Single Source Diselenoether Precursors, Chem. Mater. 24 (2012) 4442–4449. https://doi.org/10.1021/cm302864x.

[34] S.L. Benjamin, C.H. (Kees) de Groot, C. Gurnani, A.L. Hector, R. Huang, K. Ignatyev, W. Levason, S.J. Pearce, F. Thomas, G. Reid, Area Selective Growth of Titanium Diselenide Thin Films into Micropatterned Substrates by Low-Pressure Chemical Vapor Deposition, Chem. Mater. 25 (2013) 4719–4724. https://doi.org/10.1021/cm402422e.

[35] S.L. Benjamin, C.H. (Kees) de Groot, C. Gurnani, A.L. Hector, R. Huang, E. Koukharenko, W. Levason, G. Reid, Controlling the nanostructure of bismuth telluride by selective chemical vapour deposition from a single source precursor, J. Mater. Chem. A. 2 (2014) 4865. https://doi.org/10.1039/c4ta00341a.

[36] S.L. Benjamin, C.H. de Groot, A.L. Hector, R. Huang, E. Koukharenko, W. Levason, G. Reid, Chemical vapour deposition of antimony chalcogenides with positional and orientational control: precursor design and substrate selectivity, J. Mater. Chem. C. 3 (2015) 423–430. https://doi.org/10.1039/C4TC02327G.

[37] S.L. Benjamin, C.H. (Kees) de Groot, C. Gurnani, S.L. Hawken, A.L. Hector, R. Huang, M. Jura, W. Levason, E. Reid, G. Reid, S.P. Richards, G.B.G. Stenning, Compositionally tunable ternary Bi 2 (Se 1−x Te x) 3 and (Bi 1−y Sb y) 2 Te 3 thin films via low pressure chemical vapour deposition, J. Mater. Chem. C. 6 (2018) 7734–7739. https://doi.org/10.1039/C8TC01285G.

[38] R. Huang, S.L. Benjamin, C. Gurnani, Y. Wang, A.L. Hector, W. Levason, G. Reid, C.H. (Kees) De Groot, Nanoscale arrays of antimony telluride single crystals by selective chemical vapor deposition, Sci. Rep. 6 (2016) 27593. http://dx.doi.org/10.1038/srep27593.

[39] ICSD: Inorganic Crystal Structure Database (ICSD), Fachin- formationszentrum Karlsruhe (FIZ), accessed via the EPSRC National Chemical Database Service hosted by the Royal Society of Chemistry., (n.d.).

[40] T. Zhu, L. Hu, X. Zhao, J. He, New Insights into Intrinsic Point Defects in V 2 VI 3 Thermoelectric Materials, Adv. Sci. 3 (2016) 1600004. https://doi.org/10.1002/advs.201600004.

[41] L. Hu, T. Zhu, X. Liu, X. Zhao, Point Defect Engineering of High-Performance Bismuth-Telluride-Based Thermoelectric Materials, Adv. Funct. Mater. 24 (2014) 5211–5218. https://doi.org/10.1002/adfm.201400474.

[42] L.D. Zhao, B.-P. Zhang, J.-F. Li, H.L. Zhang, W.S. Liu, Enhanced thermoelectric and mechanical properties in textured n-type Bi2Te3 prepared by spark plasma sintering, Solid State Sci. 10 (2008) 651–658. https://doi.org/10.1016/j.solidstatesciences.2007.10.022.

[43] G. Tan, L.-D. Zhao, M.G. Kanatzidis, Rationally Designing High-Performance Bulk Thermoelectric Materials, Chem. Rev. 116 (2016) 12123–12149. https://doi.org/10.1021/acs.chemrev.6b00255.

[44] L.-D. Zhao, S.-H. Lo, Y. Zhang, H. Sun, G. Tan, C. Uher, C. Wolverton, V.P. Dravid, M.G. Kanatzidis, Ultralow thermal conductivity and high thermoelectric figure of merit in SnSe crystals, Nature. 508 (2014) 373–377. https://doi.org/10.1038/nature13184.

[45] Y. Pan, J.F. Li, Thermoelectric performance enhancement in n-type Bi2(TeSe)3 alloys owing to nanoscale inhomogeneity combined with a spark plasma-textured microstructure, NPG Asia Mater. 8 (2016) e275-8. https://doi.org/10.1038/am.2016.67.

[46] J.P. Heremans, B. Wiendlocha, A.M. Chamoire, Resonant levels in bulk thermoelectric semiconductors, Energy Environ. Sci. 5 (2012) 5510–5530. https://doi.org/10.1039/C1EE02612G.

[47] G.J. Snyder, E.S. Toberer, Complex thermoelectric materials, Nat. Mater. 7 (2008) 105–114. https://doi.org/10.1038/nmat2090.

[48] A.F. May, J.-P. Fleurial, G.J. Snyder, Thermoelectric performance of lanthanum telluride produced via mechanical alloying, Phys. Rev. B. 78 (2008) 125205. https://doi.org/10.1103/PhysRevB.78.125205.

[49] A.F. May, D.J. Singh, G.J. Snyder, Influence of band structure on the large thermoelectric performance of lanthanum telluride, Phys. Rev. B. 79 (2009) 153101. https://doi.org/10.1103/PhysRevB.79.153101.

[50] M. Cutler, J.F. Leavy, R.L. Fitzpatrick, Electronic Transport in Semimetallic Cerium Sulfide, Phys. Rev. 133 (1964) A1143–A1152. https://doi.org/10.1103/PhysRev.133.A1143.

[51] F. Yu, J. Zhang, D. Yu, J. He, Z. Liu, B. Xu, Y. Tian, Enhanced thermoelectric figure of merit in nanocrystalline Bi2Te3 bulk, J. Appl. Phys. 105

(2009) 094303. https://doi.org/10.1063/1.3120865.

[52] Z. Chen, X. Zhang, Y. Pei, Manipulation of Phonon Transport in Thermoelectrics, Adv. Mater. 30 (2018) 1705617. https://doi.org/10.1002/adma.201705617.

[53] X. Zhou, Y. Yan, X. Lu, H. Zhu, X. Han, G. Chen, Z. Ren, Routes for high-performance thermoelectric materials, Mater. Today. 21 (2018) 974–988. https://doi.org/10.1016/j.mattod.2018.03.039.

[54] H.-S. Kim, Z.M. Gibbs, Y. Tang, H. Wang, G.J. Snyder, Characterization of Lorenz number with Seebeck coefficient measurement, APL Mater. 3 (2015) 041506. https://doi.org/10.1063/1.4908244.